

Basin-Mode Interactions and Selection by the Mean Flow in a Reduced-Gravity Quasigeostrophic Model

MAHDI BEN JELLOUL

Laboratoire d'Océanographie Dynamique et de Climatologie, Université Pierre et Marie Curie, Paris, France

THIERRY HUCK

Laboratoire de Physique des Océans, CNRS, Brest, France

(Manuscript received 19 August 2002, in final form 9 April 2003)

ABSTRACT

The selection mechanisms of Rossby basin modes are investigated in the reduced-gravity quasigeostrophic framework. The linear solution of the wind-driven circulation is decomposed in a steady forced-dissipated solution and a time-dependent component. The steady solution consists in a classical Sverdrup flow dissipated in a thin western boundary layer. The time-dependent solution is a sum of Rossby basin modes with arbitrary amplitudes. The effect of the nonlinear term is handled through a weakly nonlinear analysis providing a set of evolution equations for the mode amplitudes. It is shown both analytically (infinite Burger number) and numerically (finite Burger number) that mode stability is related to the gyre configuration. For cyclonic or anticyclonic single gyres, all basin modes are neutral. In the traditional (reversed) double-gyre case, large-scale basin modes are damped (unstable). Pure basin-mode interactions yield triads with cycling energy and subharmonic instabilities. The latter provide a potential mechanism for spectral reddening.

1. Introduction

Historical oceanic data analysis (Kushnir 1994; Mann et al. 1998; and many others) provides evidence of interannual to interdecadal variability that is also found in coupled (Delworth et al. 1993) and ocean (Greatbatch and Zhang 1995; Colin de Verdière and Huck 1999; Delworth and Greatbatch 2000) general circulation models. Because of their global spatial pattern and their decadal timescales, baroclinic Rossby basin modes supply a plausible explanation for these variability signals: these are westward-propagating Rossby waves reinitiated at the eastern boundary through rapid Kelvin wave adjustment processes.

In the inviscid case, all basin modes are equally neutral independent of their spatial scale in the absence of a mean circulation. Cessi and Primeau (2001) argue that stochastic (white noise) atmospheric forcing equally excites basin modes but only the low-frequency part of the spectrum emerges because of the dissipation: low-frequency modes are the large-scale modes that are less dissipated and thus more resonant.

Adopting a dynamical system approach of the wind-

driven circulation, Dijkstra (2000), among others, shows that basin modes emerge through a Hopf bifurcation of the steady circulation when the dissipation to stationary forcing ratio is lowered. Unstable modes fed by the mean flow appear to be an alternative candidate mechanism for the low-frequency variability. Our aim is to provide some analytical exploration of mode selection through this type of mechanism.

For this purpose, we apply standard nonlinear physics techniques to investigate the nonlinear interaction involving basin modes and the wind-driven circulation. We treat the simple academic case of a quasigeostrophic (QG) homogeneous reduced-gravity ocean forced by a time-independent wind stress in a closed basin (section 2). Actually, more than one active layer is necessary for a better description of the wind-driven ocean circulation. Here we restrict ourselves to the one-layer case to assess the suitability of the nonlinear techniques that we use and postpone examination of more realistic multilayer model to future work. Furthermore, this is a simple way to inhibit energetic mesoscale baroclinic instability.

Following a weakly nonlinear expansion, we are able to decompose the flow in a sum of a steady component verifying the Sverdrup balance and a series of normal basin modes whose amplitudes remain arbitrary at this first stage of the expansion (section 3). Analytical solutions are available in the infinite Burger number limit (Longuet-Higgins 1964; Pedlosky 1987) but are com-

Corresponding author address: Thierry Huck, Laboratoire de Physique des Océans, Université de Bretagne Occidentale, UFR Sciences, 6 avenue Le Gorgeu, BP 809, 29285 Brest CEDEX, France.
E-mail: thuck@univ-brest.fr

puted numerically otherwise, with emphasis on weak dissipation to promote the dispersion term, in contrast to Cessi and Primeau (2001). The nonlinear interactions are investigated through amplitude equations, which are ordinary differential equations resulting from resonance elimination at the next order of the expansion (sections 4 and 5). Both basin-mode/steady flow and multimodal interactions will be addressed. Interesting differences between interactions with single and double gyres are found. Nonlinear cubic saturation is briefly evoked in section 6, before we conclude and discuss the principal results of this study (section 7).

2. Formulation

As a simple model of the upper-ocean circulation in a closed basin, we consider the reduced-gravity quasi-geostrophic potential vorticity equation. The forcing is provided by the curl of the wind stress τ , and the dissipation \mathcal{F} is, for now, arbitrary. The evolution equation for the streamfunction ψ ($\text{m}^2 \text{s}^{-1}$) is

$$\begin{aligned} \partial_t(\nabla^2\psi - R_d^{-2}\psi) + \beta\partial_x\psi + J(\psi, \nabla^2\psi) \\ = (\rho_0 H)^{-1} \text{curl}\tau + \mathcal{F}, \end{aligned} \tag{1}$$

where $R_d = \sqrt{g'H/f_0}$ is the baroclinic Rossby radius of deformation, g' is the reduced-gravity parameter, H is the upper-layer thickness, ρ_0 is the seawater density, f_0 is the local value of the Coriolis parameter, and β is its meridional gradient. Using the following adimensionalization,

$$\begin{aligned} (x, y) \rightarrow L_x(x, y), \quad t \rightarrow (\beta L_x)^{-1}t, \\ \psi \rightarrow \tau_0(\rho_0 H \beta)^{-1}\psi, \end{aligned} \tag{2}$$

where L_x is the zonal width of the basin, the nondimensional quasigeostrophic evolution equation reads

$$\partial_t(\nabla^2\psi - \text{Bu}^{-1}\psi) + \beta\partial_x\psi + \epsilon J(\psi, \nabla^2\psi) = W_E + \mathcal{F}, \tag{3}$$

where the Ekman pumping W_E is a function with maximum amplitude of 1 and \mathcal{F} are the weak dissipative processes. Additional nondimensional parameters are the Burger number Bu and a small parameter $\epsilon \ll 1$ controlling the inertial nonlinearities:

$$\text{Bu} = \frac{R_d^2}{L_x^2} \quad \text{and} \quad \epsilon = \frac{\tau_0}{\rho_0 H \beta^2 L_x^3}. \tag{4}$$

The nondimensional parameter $\beta = O(1)$ is kept to track the origin of the term involved in the algebra of the following sections. No normal flow at the boundaries and mass conservation constraint are used (McWilliams 1977; Flierl 1977):

$$\forall \mathbf{x} \in \partial\mathcal{D} \quad \text{and} \quad \psi(\mathbf{x}) = \psi_b(t),$$

such that

$$\iint_{\mathcal{D}} dx dy \psi = 0. \tag{5}$$

The spatial domain of integration \mathcal{D} is rectangular with an aspect ratio denoted by $r = L_y/L_x$. This mass-conserving condition (vs the traditional but incorrect $\psi = 0$ boundary condition) is crucial to the existence of weakly damped large-scale modes in the presence of dissipation (Cessi and Primeau 2001). However, the traditional boundary condition is correct in the particular case of infinite Burger number in which the mass-conserving condition is relaxed.

We solve this equation by a weakly nonlinear expansion (Nayfeh 1993) for ψ of the form

$$\psi = \psi_0 + \epsilon\psi_1 + \epsilon^2\psi_2 + \dots, \tag{6}$$

assuming a multiple-timescale expansion

$$\partial_t = \partial_{t_0} + \epsilon\partial_{t_1} + \epsilon^2\partial_{t_2} + \dots. \tag{7}$$

3. Rossby basin modes on a background stationary Sverdrup flow

a. Stationary solution

Averaging the first-order evolution equation yields the steady-state solution

$$\beta\partial_x\bar{\psi}_0 = W_E + \mathcal{F}, \tag{8}$$

where the overbar denotes averaging over all timescales t_i . The solution is composed of an inviscid Sverdrup interior circulation and a thin western boundary current where dissipation is active. Some friction, whatever its type, is needed to dissipate the potential vorticity input: this occurs in a western boundary layer the thickness of which is controlled by the dissipation coefficient. For instance, for Rayleigh friction ($\mathcal{F} = -\mu\nabla^2\psi$), Stommel boundary layer width scales as μ/β , while for Laplacian friction ($\mathcal{F} = A\nabla^4\psi$), a Munk boundary layer width scales as $(A/\beta)^{1/3}$. In the following, we assume, except when specifically mentioned, that dissipation is strong enough to have a western boundary current that is well described by a linear solution. This condition is equivalent to having a boundary current width larger than the inertial length $(U/\beta)^{1/2}$, where $U = \tau_0(\rho_0 H \beta L_x)^{-1}$ is a measure of the Sverdrup flow strength (Pedlosky 1996). Moreover, the basin zonal width is assumed to be sufficiently large in comparison with the western boundary layer thickness. These two theoretical assumptions mean that our Sverdrup circulation can always be closed with a linear western boundary current for any arbitrary weak dissipation by just requiring sufficiently large L and/or sufficiently small τ_0 . Using these assumptions one can write

$$\bar{v}_0 = \partial_x\bar{\psi}_0 = \beta^{-1}W_E - \beta^{-1}\delta(x) \int_0^1 dx W_E, \tag{9}$$

where δ is the Dirac distribution and represents the strongly localized western boundary current. The streamfunction is, thus,

$$\bar{\psi}_0 = \beta^{-1}W_E[x - H(x)], \tag{10}$$

where $H(x)$ is the Heaviside function. Note that this singular solution can be obtained by taking the limit of zero dissipation in the classical expressions of Stommel and Munk boundary currents (e.g., Pedlosky 1996, 36–42).

b. Basin modes

Since we have seen in the previous section that dissipation can be taken as small as possible, provided the basin scale is sufficiently large, we can neglect it at this order. The time-dependent component of (3) is then

$$\mathcal{L}\tilde{\psi}_0 = \partial_{t_0}(\nabla^2\tilde{\psi}_0 - \text{Bu}^{-1}\tilde{\psi}_0) + \beta\partial_x\tilde{\psi}_0 = 0, \quad (11)$$

which solutions are the Rossby basin modes. Neglecting the dissipation at this order of the expansion results in useful properties that would be absent in the presence of dissipation. Moreover, inserting dissipation at this order would lead us to rapidly, that is, over rapid timescale t_0 , damped modes. We provide in the following a mathematical formulation suitable for the weakly non-linear analysis conducted in the next sections.

Equation (11) can be rewritten

$$\partial_{t_0}\tilde{\psi}_0 = \mathcal{A}\tilde{\psi}_0 = -Q^{-1}\beta\partial_x\tilde{\psi}_0, \quad (12)$$

where the linear operators Q and \mathcal{A} are defined by

$$Qf = \nabla^2f - \text{Bu}^{-1}f \quad \text{and} \quad \mathcal{A} = -Q^{-1}\beta\partial_x. \quad (13)$$

Defining

$$\begin{aligned} \langle f | g \rangle_Q &= -\frac{1}{2r} \iint_D dx dy f Qg \\ &= \frac{1}{2r} \iint_D dx dy (\nabla f \cdot \nabla g + \text{Bu}^{-1}fg) \\ &\quad + \frac{1}{2r} \oint_{\partial D} ds f(\mathbf{n} \cdot \nabla g) \end{aligned} \quad (14)$$

provides a scalar product for the space of real functions verifying (5) if the last contour integral is zero. The streamfunction being a function of time only on the boundaries, this contour integral can be rewritten

$$\begin{aligned} \oint_{\partial D} ds f(\mathbf{n} \cdot \nabla g) &= f \oint_{\partial D} ds(\mathbf{n} \cdot \nabla g) \\ &= f \oint_{\partial D} ds u_g, \end{aligned} \quad (15)$$

where $u_g = (-\partial_y g, \partial_x g)$: this last circulation vanishes for every solution of (11) as pointed out by Pedlosky (1987, p. 145).

Thus in the space of zero circulation streamfunction, the operator \mathcal{A} is anti-Hermitian for the metric defined by the scalar product (14); that is,

$$\langle f | \mathcal{A}g \rangle_Q = \langle \mathcal{A}^*f | g \rangle_Q = -\langle \mathcal{A}f | g \rangle_Q, \quad (16)$$

where the dagger denotes adjoint operators. The operator \mathcal{A} is thus diagonal in a base of orthonormal complex eigenvectors Φ_Ω with pure imaginary eigenvalues $i\Omega$ composing a discrete spectrum verifying

$$\partial_{t_0}\Phi_\Omega = \mathcal{A}\Phi_\Omega = i\Omega\Phi_\Omega. \quad (17)$$

We can thus conclude about the purely oscillating nature of the basin modes on timescale t_0 and write the time-dependent solution

$$\tilde{\psi}_0 = \sum_{\Omega \in \mathcal{S}_A} [A_0(\Omega, t_1, \dots)\Phi_\Omega(x, y)e^{i\Omega t_0} + \text{c.c.}], \quad (18)$$

where c.c. denotes the complex conjugate of the first term in the bracket and \mathcal{S}_A is the spectrum of positive (or negative) discrete frequencies.

Since $\tilde{\psi}_0$ is a real function, the relation $A_0(-\Omega) = A_0^*(\Omega)$ holds and the sum is thus restricted to positive Ω . The eigenmodes Φ_Ω verify the linear relation

$$\mathcal{L}\Phi_\Omega = i\Omega(\nabla^2\Phi_\Omega - \text{Bu}^{-1}\Phi_\Omega) + \beta\partial_x\Phi_\Omega = 0, \quad (19)$$

which is strictly equivalent to (17); they are uniquely defined provided the following energy normalization:

$$\frac{1}{2r} \iint_D dx dy (|\nabla\Phi_\Omega|^2 + \text{Bu}^{-1}|\Phi_\Omega|^2) = 1. \quad (20)$$

The time-dependent vectors $(\Phi_\Omega e^{i\Omega t_0} + \text{c.c.})$ thus form an orthonormal base of the kernel of the anti-Hermitian operator \mathcal{L} for the space–(fast) time scalar product

$$\langle f | g \rangle = \frac{1}{2r} \lim_{T_0 \rightarrow \infty} \frac{1}{T_0} \int_0^{T_0} dt_0 \iint_D dx dy fg. \quad (21)$$

This property will be used in section 4 to obtain the slow time evolution equations for the amplitude $A_0(\Omega, t_1)$.

1) NO-SURFACE-DEVIATION CASE

The simple case of no surface deviation (rigid lid), that is, $\text{Bu}^{-1} = 0$, is treated in the Longuet-Higgins (1964) classical paper and Pedlosky (1987) textbook. The analytical solution is

$$\Phi_\Omega = D_\Omega e^{i\beta x/2\Omega} \sin(m\pi x) \sin\left(\frac{n\pi y}{r}\right), \quad (22a)$$

with

$$D_\Omega = \frac{4\Omega}{\beta} \quad \text{and} \quad \Omega = \frac{\beta}{2\pi\sqrt{m^2 + n^2r^{-2}}}. \quad (22b)$$

2) GENERAL CASE

In the general case with finite Burger number, we proceed by numerically computing the modes. We solve the generalized eigenvalue problem arising after finite differentiating (19), like Cessi and Primeau (2001):

TABLE 1. Basin modes' period as a function of their spatial structure for different values of the Burger number Bu ($r = 1$). Wavenumbers are indicated using the scheme (*zonal* \times *meridional*) by counting the maxima of the streamfunction modulus (envelope) $|\Phi_\Omega|$, providing a direct connection with the frictionless infinite Burger analytical solution. The periods corresponding to these modes are also indicated: the time unit is the time needed for the largest Rossby wave to cross the basin, that is; $T_R = L_c/(\beta R_\beta^2)$. For the temporal scaling used in the text, periods must be multiplied by Bu^{-1} . Values are given for the lowest achievable dissipation ($\delta = 10^{-4}$ to 10^{-5}) given our limited 100×100 resolution. Convergence for the eigenvalues is obtained up to 10^{-3} to 10^{-4} .

Bu	∞	1	10^{-2}	10^{-4}	Bu	∞	1	10^{-2}
1×1	55.8	57.6	1.372	1.033	1×2	88.3	90.6	1.54
2×1	88.3	90.3	1.540	0.522	2×2	111.7	116.2	1.69
3×1	124.8	129.5	1.715	0.355	3×2	142.3	146.3	1.91
4×1	162.8	167.1	1.980	0.274	4×2	176.6	182.1	2.29

$$i\Omega(\nabla^2\Phi_\Omega - Bu^{-1}\Phi_\Omega) = -\beta\partial_x\Phi_\Omega + \delta\nabla^2(\nabla^2\Phi_\Omega - Bu^{-1}\Phi_\Omega), \quad (23)$$

using Arnoldi's method provided in ARPACK (Lehouck et al. 1998). Downgradient potential vorticity eddy diffusion is needed here to avoid gridpoint structures and to numerically isolate large-scale modes.

The transition from two asymptotic regimes depending on the value of the Burger number clearly appears in Table 1. These two regimes depend on the ratio of dispersive to advective terms, as shown by a simple scaling of (23):

- high Bu: low-frequency modes are small-scale modes ($\Omega \propto 1/\sqrt{m^2 + r^{-2}n^2}$);
- small Bu: low-frequency modes are large-scale modes ($\Omega \propto m$), as noted by Cessi and Primeau (2001).

This latter case is the most oceanographically relevant since thermocline evolution is well captured by the first baroclinic mode for which $Bu \ll 1$. A few of these modes are represented in Fig. 1: in comparison with the infinite Burger number analytical solution, their meridional structure is primarily uniform except for north and south boundary layers. For values of our parameters

typical of the North Atlantic and Pacific, these modes have periods in the interannual to interdecadal range.

4. Nonlinear instability mechanism

a. Amplitude equation

We proceed to the next order in the weakly nonlinear expansion to include the nonlinear terms in (3) that were neglected at first order. This provides the slow evolution equation for the amplitudes of the basin modes.

At $O(\epsilon)$, the evolution equation reads

$$\mathcal{L}\psi_1 = -[\partial_{t_1}Q\psi_0 + J(\psi_0, \nabla^2\psi_0)]. \quad (24)$$

Amplitude equations are obtained as a solvability condition for (24): by left multiplication of both sides of (24) by the elements of the kernel of $\mathcal{L}^\dagger = -\mathcal{L}$ and recalling (19), we get

$$\begin{aligned} \langle \Phi_\Omega | \mathcal{L}\psi_1 \rangle &= \langle \mathcal{L}^\dagger\Phi_\Omega | \psi_1 \rangle = -\langle \mathcal{L}\Phi_\Omega | \psi_1 \rangle = 0 \\ &= -\langle \Phi_\Omega | \partial_{t_1}Q\psi_0 + J(\psi_0, \nabla^2\psi_0) \rangle. \end{aligned} \quad (25)$$

Then we expand $\psi_0 = \bar{\psi}_0 + \tilde{\psi}_0$ using (18). The scalar products are evaluated using the normalization condition (20) and the identity $A_0(-\Omega) = A_0^*(\Omega)$. For $\Omega = \Omega_0$, this prescription yields

$$\begin{aligned} \partial_{t_1}A_0(\Omega_0) &= \sum_{\Omega_1, \Omega_2 \in \mathcal{S}_a} \left[\delta_{\Omega_0, \Omega_1 + \Omega_2} A_0(\Omega_1) A_0(\Omega_2) (2r)^{-1} \iint_D dx dy \Phi_{\Omega_0}^* J(\Phi_{\Omega_1}, \nabla^2\Phi_{\Omega_2}) \right] \\ &+ A_0(\Omega_0) (2r)^{-1} \iint_D dx dy \Phi_{\Omega_0}^* [J(\Phi_{\Omega_0}, \nabla^2\bar{\psi}_0) + J(\bar{\psi}_0, \nabla^2\Phi_{\Omega_0})], \end{aligned} \quad (26)$$

where δ is the Kronecker symbol. Three types of ‘‘three wave’’ resonance can thus occur:

- self-interaction of a mode via the mean flow ($\Omega_0 + 0 = \Omega_0$),
- triad of distinct modes ($\Omega_1 + \Omega_2 = \Omega_0$),
- subharmonic interaction ($\Omega_1 + \Omega_1 = \Omega_0$).

Each case will now be examined individually. The first case will be treated at length in the following, while the

two others are postponed to the study of the interaction between distinct basin modes discussed in the next sections.

b. Basin mode: Sverdrup flow interaction

We first derive an amplitude evolution equation considering only one mode interacting with the stationary mean flow:

$$\partial_{t_1} A_0(\Omega) = a_1 A_0(\Omega), \quad (27)$$

where the complex coefficient a_1 reads from (26):

$$\begin{aligned} a_1 &= a'_1 + a''_1 \\ &= (2r)^{-1} \iint_{\mathcal{D}} dx dy [\nabla^2 \bar{\psi}_0 J(\Phi_{\Omega}^*, \Phi_{\Omega}) \\ &\quad + \bar{\psi}_0 J(\nabla^2 \Phi_{\Omega}, \Phi_{\Omega}^*)]. \quad (28) \end{aligned}$$

The imaginary part of the coefficient a_1 corresponds to a small correction to the mode frequency due to its interaction with the stationary flow. The real part is the growth rate of the mode and indicates the mode stability [$\Re(a_1) \leq 0$] or instability [$\Re(a_1) > 0$].

The first term in (28) is purely imaginary. Using (19), the second one is rewritten

$$\begin{aligned} a''_1 &= i(2r\Omega)^{-1} \iint_{\mathcal{D}} dx dy \bar{\psi}_0 J(\beta \partial_x \Phi_{\Omega}, \Phi_{\Omega}^*) \\ &\quad + (2rBu)^{-1} \iint_{\mathcal{D}} dx dy \bar{\psi}_0 J(\Phi_{\Omega}, \Phi_{\Omega}^*) \\ &= i(2r\Omega)^{-1} \iint_{\mathcal{D}} dx dy \bar{\psi}_0 J(\beta \partial_x \Phi_{\Omega}^*, \Phi_{\Omega}) \\ &\quad + (2rBu)^{-1} \iint_{\mathcal{D}} dx dy \bar{\psi}_0 J(\Phi_{\Omega}, \Phi_{\Omega}^*) \\ &\quad - i(2r\Omega)^{-1} \iint_{\mathcal{D}} dx dy \beta \partial_x \bar{\psi}_0 J(\Phi_{\Omega}, \Phi_{\Omega}^*), \quad (29) \end{aligned}$$

where the last expression was achieved using integration by parts. The complex number a_1 has no real part unless the following integral is nonzero:

$$\begin{aligned} 2\Re(a_1) &= a'_1 + \text{c.c.} \\ &= -i(2r\Omega)^{-1} \iint_{\mathcal{D}} dx dy \beta \partial_x \bar{\psi}_0 J(\Phi_{\Omega}, \Phi_{\Omega}^*). \quad (30) \end{aligned}$$

c. No-surface-deviation case

We evaluate the Jacobian in (30) using the analytical expression for the modes computed in the case of no surface deviation (22a):

$$J(\Phi_{\Omega}, \Phi_{\Omega}^*) = \frac{i\beta n \pi D_{\Omega}^2}{4r\Omega} (1 - \cos 2m\pi x) \sin \frac{2n\pi y}{r}. \quad (31)$$

Assuming a forcing $W_E(y) = \beta \partial_x \bar{\psi}_0$ independent of x , the growth rate is then

$$\begin{aligned} \Re(a_1) &= \frac{a_1 + \text{c.c.}}{2} \\ &= \frac{\beta n \pi D_{\Omega}^2}{16\Omega^2 r^2} \int_0^r dy W_E(y) \sin \frac{2n\pi y}{r}. \quad (32) \end{aligned}$$

The last expression provides indication on the nature of the instability. It appears that potentially growing modes have a meridional scale 2 times as large as the mean Sverdrup flow. We examine in the following the two classical cases of the single and double gyres.

1) SINGLE GYRE

Considering a typical single-gyre forcing $W_E = W_0 \sin \pi y/r$, with $W_0 > 0$ ($W_0 < 0$) for a subpolar cyclonic (subtropical anticyclonic) gyre, one can easily compute $a_1 = 0$. The modes are thus marginally stable in the single-gyre case. More generally, all forcings that are even functions of the latitude deviation from the mid-basin latitude $r/2$ are neutral. Only odd contributions may have destabilizing effects. Moreover $\Im(a_1) = 0$ such that no frequency shifts, due to the interaction with the mean flow, are experienced by the modes for the symmetric single gyre considered here. Note that in practice neutral modes are damped by the weak dissipative processes.

2) DOUBLE GYRE

Now, considering a traditional double-gyre symmetric forcing $W_E = -W_0 \sin(2\pi y/r)$, $W_0 > 0$, the growth rate is then

$$\Re(a_1) = -\frac{\beta \pi D_{\Omega}^2 W_0 \delta_{n,1}}{32r\Omega^2} = -\frac{W_0 \pi}{2r\beta} \delta_{n,1}. \quad (33)$$

The basin modes with largest latitudinal extension ($n = 1$) are thus damped but all other modes are marginally stable. However, for $W_0 < 0$, that is, an anticyclonic subpolar gyre north of a cyclonic subtropical gyre, these modes become unstable. This latter case presents a latitudinal gradient of relative potential vorticity opposed to the planetary gradient (Fig. 2). These opposing gradients can only “be seen” by the largest basin modes in latitude.

3) ROLE OF A FINITE-WIDTH WESTERN BOUNDARY CURRENT

So far we have crudely represented the western boundary current by a delta function in the expression of the meridional velocity in (9). It appears that the latter plays no role in determining the mode stability since its contribution is proportional to

$$\int_0^1 dx \delta(x) (1 - \cos 2m\pi x) = 1 - \cos 0 = 0. \quad (34)$$

We can allow a finite width by changing the delta function into $f(\Delta^{-1}x)/\Delta$ where the function f verifying $\int_0^{\infty} du f(u) = 1$ reflects the boundary current structure and Δ is its width. For example, the Stommel solution corresponds to a function $f(\Delta^{-1}x) = e^{-|x|/\Delta}$, where $\Delta = \mu/\beta$ and μ is the bottom friction coefficient.

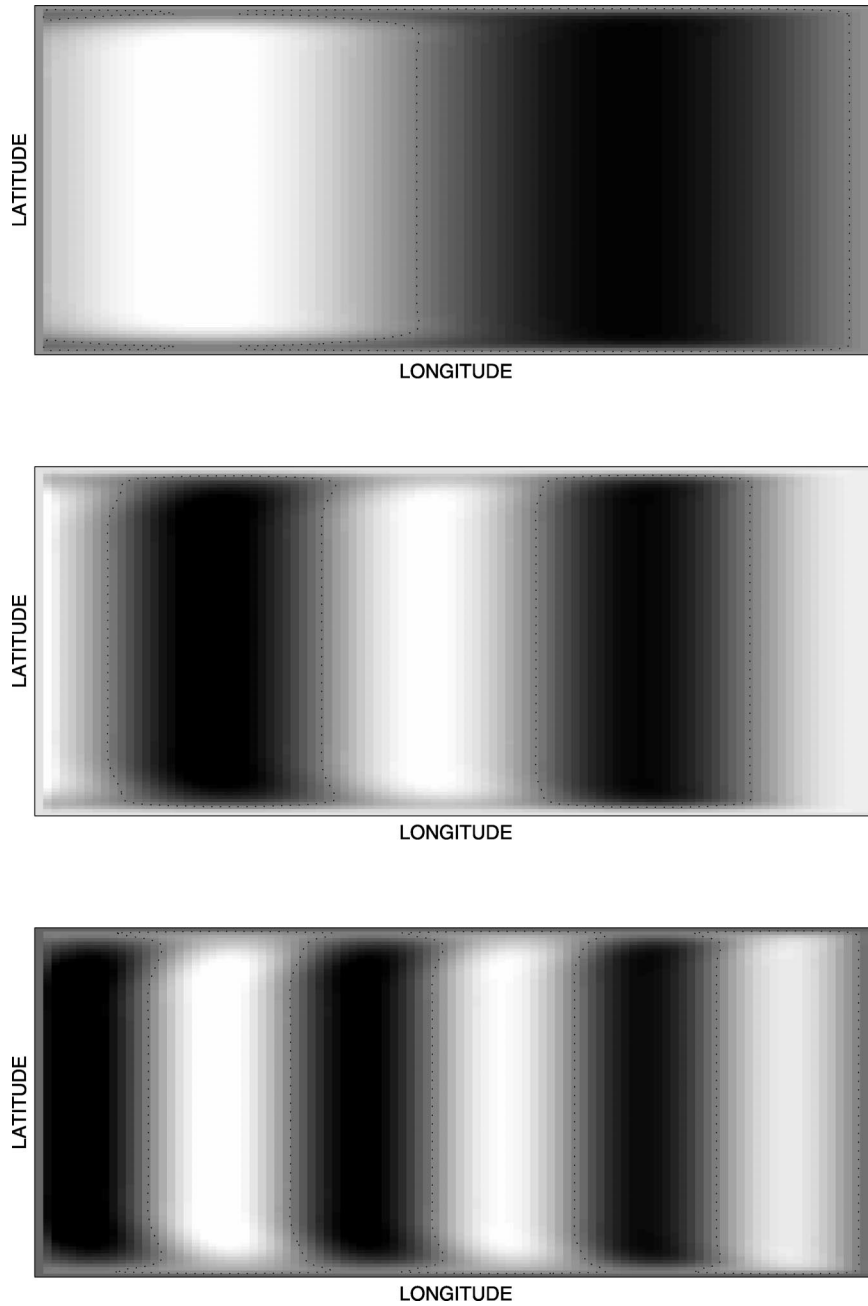


FIG. 1. Streamfunction for reduced-gravity basin modes for $Bu = 10^{-4}$ ($r = 1$, $\delta = 10^{-3}$). Zonal wavenumbers $m = 1, 2$, and 3 are represented for meridional wavenumber $n = 1$. Their periods are approximately T_R/m , where $T_R = L_x/(\beta R_d^2)$ is the dimensional time needed by the largest Rossby wave to cross the basin (this is about 10 years with typical values for the North Atlantic).

For a finite-width western boundary current, the last term reads

$$\int_0^1 dx \frac{f(x/\Delta)}{\Delta} (1 - \cos 2m\pi x), \quad (35)$$

and yields for a Stommel western boundary current

$$\begin{aligned} & \int_0^1 dx \Delta^{-1} e^{-x/\Delta} (1 - \cos 2m\pi x) \\ &= 1 - \frac{1 - e^{-\Delta^{-1}}}{1 + 4\Delta^2 m^2 \pi^2 e^{-\Delta^{-1}}}, \end{aligned} \quad (36)$$

The contribution of the western boundary current term

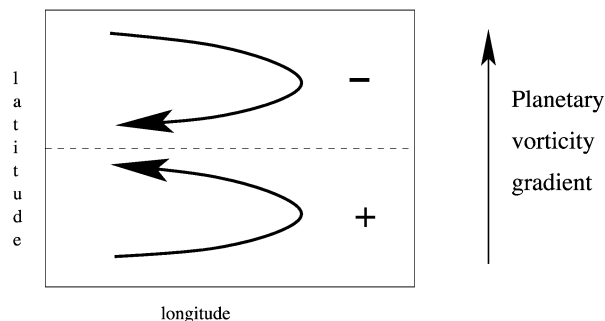


FIG. 2. Reversed double gyre leading to large-scale mode instability. Plus and minus denote the sign of the relative vorticity of the Sverdrup gyres.

can thus be as small as needed by requiring a sufficiently thin current, that is, $\Delta \ll 1$ for any fixed zonal wave-number m . Now for Δ fixed to a finite value, one can evaluate the growth rate for the double-gyre case using (30) and get the correction to (33):

$$\Re(a_1) = -\frac{W_0 \pi}{2r\beta} \frac{1 - e^{-\Delta^{-1}}}{1 + 4\Delta^2 m^2 \pi^2 e^{-\Delta^{-1}}} \delta_{n,1}. \quad (37)$$

For small-scale modes, that is, large m , the growth rate tends to vanish and the modes are thus quasi neutral. A possible explanation is that the gyre alternation is opposed in the boundary current and the Sverdrup interior. They thus may compensate when the small-scale basin mode can sample the western boundary current.

d. General case

In the general case, analytical solutions for the basin modes are missing and these can only be computed numerically. Apart from some simple cases in which symmetry arguments can be used, the growth rate has to be numerically evaluated using (30).

Let us first show that the problem's symmetries make the quantity $J(\Phi_\Omega, \Phi_\Omega^*)$ an odd function of the latitude deviation from the midbasin. Since the modes equation (11) is invariant through mirror symmetry about the midbasin longitude line $y = r/2$, if $\Phi_\Omega(x, y)$ is a solution, then $\Phi_\Omega(x, r - y)$ is also a solution. Moreover, there is no reason for the operator \mathcal{A} to be degenerate, and so two symmetric solutions must be linked as follows:

$$\Phi_\Omega(x, y)e^{i\Omega_0} + \text{c.c.} = \alpha[\Phi_\Omega(x, r - y)e^{i\Omega_0} + \text{c.c.}]. \quad (38)$$

Now, using $\Phi_\Omega^*(x, y) = \Phi_{-\Omega}(x, y)$ and taking the complex conjugate of the relation (38) yields $\alpha = \alpha^*$. Since the normalization condition implies $|\alpha| = 1$, we can thus conclude that $\alpha = \pm 1$. The eigenmodes $\Phi_\Omega(x, y)$ are thus odd or even functions of the latitude deviation from the midbasin.

TABLE 2. Growth rate for basin modes interacting with idealized single subpolar gyre and reversed double gyre ($r = 1$). The time unit is the time needed for the largest Rossby wave to cross the basin, $T_R = L_x / (\beta R_D^2)$. For the time scaling used in the text, growth rate must be multiplied by Bu^{-1} . Values are given for the lowest achievable friction given our limited 100×100 resolution.

Gyre type	Double reversed			Single subpolar		
	Bu	∞	1	10^{-2}	∞	1
1×1	$\pi/2$	1.500	1.538	0	-0.010	-0.010
1×2	0	0.054	0.012	0	-0.056	-0.057
2×1	$\pi/2$	1.560	1.560	0	-0.011	-0.011
3×1	$\pi/2$	1.630	1.400	0	-0.012	-0.010

1) SINGLE GYRE

We first consider forcings that are even functions of the latitude deviation from the midbasin latitude $r/2$, like the simple gyre studied above. Since $J(\Phi_\Omega, \Phi_\Omega^*)$ is an odd function of the same variable, the integral (30) is clearly zero. This is verified numerically for several modes and different Burger numbers as reported in Table 2. Only odd streamfunctions may have destabilizing effects. Moreover, no frequency shift is experienced by the modes since $a_1 = \Re(a_1) = \Im(a_1) = 0$ for the even gyre considered here.

2) DOUBLE GYRE

For the double-gyre case, the growth rate is computed numerically (see Table 2). These results are comparable to those found in the no-surface-deviation case; that is, anticyclonic (cyclonic) gyre north (south) yields unstable modes with basin scales. However, the gravest modes are now low-frequency modes for small Bu. Note that the exponential growths (when rescaled by the largest Rossby wave basin crossing time) are close to the one obtained with infinite Burger number frictionless solution; that is, $\Re(a_1) = \pi/2$. We did not manage to obtain decent results for Burger numbers lower than 10^{-2} because of our limited spatial resolution of the eigenmodes and their alteration by the dissipation.

e. Instability and symmetry

As shown above, the stability properties of the gyres are related to their symmetry properties. In fact, only the nonlinearities break the symmetry $W_E \rightarrow -W_E$, $\psi \rightarrow -\psi$ of the linearized quasigeostrophic equation such that opposite configurations have different stability behavior.

A rule of thumb may be that instability develops for Sverdrup transport with mirror-antisymmetric components having anticyclonic gyre north of a cyclonic one. Consider a zonal wind forcing written as a series of sine functions:

$$W_E(y) = \sum_{k \in \mathbb{N}} S_k \sin \frac{k\pi y}{r}. \quad (39)$$

From (30) it appears that the unstable modes are the ones with latitudinal wavenumber $n = k/2$ whenever $S_k > 0$ (only even k harmonics are potentially unstable) for the case $Bu = \infty$. The unstable modes are thus 2 times as large in latitude as the Ekman pumping. This result can be easily extrapolated to the finite Bu case in which the selected mode scale is approximately 2 times the scale $k^{-1}r$ of the potentially unstable k harmonic of the forcing.

Numerical studies for both single gyre (Sheremet et al. 1997) and double gyre (Cessi and Ierley 1995; Dijkstra 2000; among others) have shown that the first instability that appears in the dissipative one-layer quasigeostrophic system when increasing the forcing-to-dissipation ratio (Reynolds number) may break the mean flow symmetry arising from a symmetric forcing. In the double-gyre case, the pitchfork bifurcation results in multiple nonsymmetric steady states departing from the classical Sverdrup flow with linear Munk- or Stommel-type boundary current.

In the single-gyre case of Sheremet et al. (1997) the lower-branch solution, which presents a boundary layer, is stable until some critical Reynolds number at which Hopf bifurcations start to occur. However no basin modes are directly involved in these instabilities, which are mainly due to wall-trapped modes. This result is confirmed by our prediction. However, for larger Reynolds number these authors found an unstable resonant mode that is mainly an oscillatory recirculating mode whose frequency matches a basin-mode frequency shifted by the mean flow.

In the double-gyre case, the pitchfork bifurcation yields two mirror-symmetric stable mean flows that are no longer symmetric with respect to the midlatitude axis. For higher Reynolds number these two stationary solutions are unstable through Hopf bifurcation and the unstable pattern is clearly related to basin modes (Dijkstra and Katsman 1997). There is no contradiction with our prediction since the unstable basin mode has a meridional wavenumber 2, while we only predicted that basin modes with meridional wavenumber 1 are damped. We may conjecture that the excitation of wavenumber 2 basin modes is due to the asymmetry of the mean flow. Although we cannot evaluate numerically the growth rate for this particular mean flow, we may argue that, within each gyre, the potential vorticity gradient related to the recirculating zone is opposed to the planetary gradient: the unstable mode thus has the largest meridional scale in each gyre. The analysis conducted here tentatively rationalizes some of these results by providing a criterion for basin-mode selection. Unfortunately, it is not suitable for the gyre mode instabilities that several authors have found (Jiang et al. 1995; Speich et al. 1995; Dijkstra and Katsman 1997; Simonnet and Dijkstra 2002).

In the following, it will be assumed that the forcing does not destabilize the basin modes at this order in ϵ . The potential destabilizing effects, like asymmetry, will be taken as sufficiently weak to be postponed to the next order (section 6).

5. Basin-mode interactions

a. Basin-mode triads

1) NO-SURFACE-DEVIATION CASE

Triadic interactions are possible for basin modes with the dispersion relation given in (22a). For example, consider the modes with frequencies $\Omega(pm, pn)$, $\Omega(qm, qn)$ and $\Omega(sm, sn)$, with (p, q, s) being a triplet of integers. The resonance condition reads

$$\frac{1}{p} + \frac{1}{q} = \frac{1}{s}, \quad (p, q, s) \in \mathbb{N}^3, \quad (40)$$

which is verified for several combinations. For such triadic interactions, we end up with the following system:

$$\partial_{t_1} A_0(\Omega_0) = a_{\Omega_0^{\Omega_1, \Omega_2}} A_0(\Omega_1) A_0(\Omega_2), \quad (41a)$$

$$\partial_{t_1} A_0(\Omega_1) = a_{\Omega_1^{\Omega_0, -\Omega_2}} A_0(\Omega_0) A_0^*(\Omega_2), \quad \text{and} \quad (41b)$$

$$\partial_{t_1} A_0(\Omega_2) = a_{\Omega_2^{\Omega_0, -\Omega_1}} A_0(\Omega_0) A_0^*(\Omega_1), \quad (41c)$$

where the $a_{\Omega_i^{\Omega_j, \Omega_k}}$ are the interaction coefficients.

These triads are just a particular case of the general Rossby wave triads since every basin mode is composed of four Rossby waves; details can be found in Pedlosky (1987). Both energy and enstrophy of the triad are conserved, and the system (41) undergoes nonlinear periodic oscillations.

2) GENERAL CASE

In the general case there is no reason for triads to occur. Moreover, considering an arbitrary basin geometry, triad occurrences are rather unlikely (nongeneric resonances). However, the case of a large basin is interesting because near-triadic resonance might occur since large-scale Rossby wave frequencies are quite insensitive to basin geometry (these waves do not feel the details of the shore). Moreover, their frequencies are multiples of $T_R^{-1} = (L_x / \beta R_D^2)^{-1}$ (see, e.g., modes 1×1 , 2×1 , and 3×1 for $Bu = 10^{-4}$ in Table 1), and thus resonance among the three largest modes may be approximately achieved. This is far beyond the scope of this paper and will not be pursued any further.

b. Subharmonic instability

1) NO-SURFACE-DEVIATION CASE

In the case of no surface deviation, the dispersion relation provides exact subharmonic resonances since $2\Omega(2m, 2n) = \Omega(m, n)$, and more generally $k\Omega(km, kn) = \Omega(m, n)$. We will restrict ourselves to the first case since we deal with quadratic nonlinearities. Using $\Omega_0 = 2\Omega_1 = 2\Omega$ we thus get

$$\partial_{t_1} A_0(\Omega) = a_{\Omega^{2\Omega, -\Omega}} A_0(2\Omega) A_0^*(\Omega), \quad (42)$$

where the complex interaction coefficient is such that

$$\begin{aligned}
a_{\Omega}^{2\Omega, -\Omega} &= (2r)^{-1} \iint_{\mathcal{D}} dx dy \Phi_{\Omega}^* J(\Phi_{2\Omega}, \nabla^2 \Phi_{\Omega}^*) + (2r)^{-1} \iint_{\mathcal{D}} dx dy \Phi_{\Omega}^* J(\Phi_{\Omega}^*, \nabla^2 \Phi_{2\Omega}) \\
&= i(2r)^{-1} \beta \Omega^{-1} \iint_{\mathcal{D}} dx dy \Phi_{2\Omega} J(\Phi_{\Omega}^*, \partial_x \Phi_{\Omega}^*).
\end{aligned} \tag{43}$$

Some tedious, but straightforward, algebra yields

$$a_{\Omega}^{2\Omega, -\Omega} = - \frac{8i\beta D_{2\Omega} D_{\Omega} \sin \frac{n\pi}{2} e^{-3i\beta/4\Omega} \left[m\pi \left(\cos \frac{m\pi}{2} - 1 \right) + \frac{3i\beta}{2\Omega} \sin \frac{m\pi}{2} \right]}{15r \left(m^2 \pi^2 - \frac{9\beta^2}{4\Omega^2} \right)}. \tag{44}$$

If we write $a_{\Omega}^{2\Omega, -\Omega} A_0(2\Omega) = R e^{i\theta}$, and change the variable $A_0(\Omega)$ to $B = A_0(\Omega) e^{-i\theta/2}$, we end up with

$$\partial_{t_1} B = RB^* - \mu B, \tag{45}$$

where a dissipative stabilizing term is required to have instability at nonzero R ; otherwise, the trivial equilibrium solution $B = 0$ of the last system is unstable for every R since the eigenvalues are $\pm R$ (e.g., Fauve 1998). Subharmonic instability is a well-known feature of quadratic nonlinear system (Strogatz 1994). For the case with no surface deviation, large-scale modes are destabilized through subharmonic instability to produce slower modes with half-scale in both zonal and meridional directions [recall the resonance condition $2\Omega(2m, 2n) = \Omega(m, n)$].

2) GENERAL CASE

For reduced-gravity modes with $Bu \approx 0$, the resonance holds for a given mode with frequency Ω_0 and its subharmonic, which is 2 times as large in the zonal direction. However, the subharmonic resonance condition is only approximately verified up to a small frequency correction $\nu = \Omega_0 - 2\Omega_1 \neq 0$ for the modes with the largest zonal wavelengths (this discrepancy is related to the small but nonzero dispersion effects). The resulting amplitude equation must then include a frequency correction term as follows:

$$\partial_{t_1} B = RB^* + i\nu B - \mu B. \tag{46}$$

The growth rate of a perturbation from the trivial steady state $B = 0$ is then

$$\sigma = -\mu + \sqrt{R^2 - \nu^2} \tag{47}$$

and may become positive for sufficiently strong R .

As an illustration, Cessi and Paparella (2001) found in their numerical simulation of a one-layer rotating shallow-water model (RSW) in a large basin (similar to our $Bu \ll 1$ case), forced by a simple interactive wind stress, a period doubling transition from mode 1×1 to mode 2×1 .

However, note that in our β -plane QG model, the basin modes must have different latitudinal structure for subharmonic instability to develop. Indeed, the formula of the coupling parameter $a_{\Omega}^{2\Omega, -\Omega}$, which was analytically computed for $Bu = \infty$ in (43) and has a similar expression in the general case, yields to $a_{\Omega}^{2\Omega, -\Omega} = 0$ when the involved modes are 1×1 and 2×1 . This cancellation occurs when the integrand is an odd function of the latitude deviation from the midbasin. For example, if the initial mode with frequency 2Ω is even, the coupling parameter is zero since the Jacobian in (43) is always odd. As a consequence, (44) yields $a_{\Omega}^{2\Omega, -\Omega} = 0$ for even n .

This point seems at odds with the Cessi and Paparella (2001) result. However, since their RSW model considers large variations of the Coriolis parameter, the speed of the fastest Rossby waves is latitude dependent (Cessi and Louazel 2001) and the modes are no longer symmetric (slanted wave fronts): therefore there is no contradiction with our symmetric case. Last, note that it is possible to include such large variations of the Coriolis parameter in a QG-like model (A. Colin de Verdière 2002, personal communication) and perform the same analysis as we provided here in the traditional β -plane QG model.

c. Summary of quadratic processes

When summed up together, the individual processes that we investigate above may lead us to the stationary spectrum of basin modes that results from the previous amplitude equations. An extensive study of these amplitude equations is far beyond the scope of this paper, but we might qualitatively describe the energy flux.

Energy input in the time-varying component of the system is provided by the mean flow (when unstable) and feeds modes with scales similar to the unstable harmonics (see section 4e). Two- and three-mode quadratic interactions distribute energy throughout the modes. The energy may then cycle through triads with no net energy input nor loss. However, there is a net energy flux toward

low frequencies through subharmonic instability. For the case with no surface deviation ($Bu = \infty$), the red part of the spectrum corresponds to modes with small spatial scales, but for the opposite limiting case ($Bu \ll 1$) it consists in the large-scale modes. The system can balance the net input of energy toward the low frequencies through dissipative processes. Since dissipation is stronger at smaller scales, the spectrum will be less red for $Bu = \infty$ as compared with $Bu \ll 1$. Nevertheless dissipation is very weak in the ocean such that mode amplitudes can be sufficiently strong and high-order terms can no longer be neglected: higher-order nonlinear processes may then saturate the spectrum.

6. Nonlinear saturation

In this section we study how mode amplitudes can saturate through self interactions (cubic nonlinearities). To shed light on the mechanism invoked in the previous section, we examine only one unstable mode interacting with the mean flow, while neither subharmonic instability nor triads are considered. We assume that all sources of instability only appear at this order where nonlinear saturation can balance them: Therefore, we consider a mode with frequency Ω whose growth rate is zero at first order ($a_1 = i|a_1|$) and energy $E_0 = |A_0(t_1)|^2$ is conserved on the slow timescale t_1 (i.e., $\partial_{t_1} E_0 = 0$). We then focus on the slower time evolution equation of the amplitude A_0 , or equivalently the energy E_0 , on timescale t_2 .

a. Nonresonant fields

To calculate the nonlinear saturation terms, we must first complete the solution of the problem at the order ϵ by computing the nonresonant component of the solution. The cubic nonlinear terms that we seek will arise from the product of $\tilde{\psi}_0$ and ψ_1 . Since no triads or subharmonic instabilities are assumed, we expect contributions only from ψ_1 terms with frequencies 2Ω and 0 because only these terms can interact resonantly with $\tilde{\psi}_0$ according to the resonance relations $2\Omega - \Omega = \Omega$ and $0 + \Omega = \Omega$; see Fauve (1998) for an example.

The following convenient notations are used for the first correction to the streamfunction:

$$\begin{aligned} \psi_1 = & \sum_{\Omega \in \mathcal{S}_x} [A_1(\Omega, t_1, \dots) \Phi_\Omega e^{i\Omega t_0} \\ & + A_1(2\Omega, t_1, \dots) \Phi_{2\Omega} e^{i2\Omega t_0} + \text{c.c.}] \\ & + \bar{\psi}_1^{t_0} + \text{n.r.t.}, \end{aligned} \quad (48)$$

where n.r.t. stands for nonresonant terms.

Averaging (24) gives

$$\beta \partial_x \bar{\psi}_1^{t_0} = -\overline{J(\psi_0, \nabla^2 \psi_0)}^{t_0}. \quad (49)$$

Then expanding $\psi_0 = \bar{\psi}_0 + \tilde{\psi}_0$ using (18) one obtains

$$\beta \partial_x \bar{\Phi}_1 = -J(\bar{\psi}_0, \nabla^2 \bar{\psi}_0) + W_{E1}^{AS} \quad \text{and} \quad (50a)$$

$$\begin{aligned} \beta \partial_x \Phi_{\Omega, \Omega^*} &= -[J(\Phi_\Omega, \nabla^2 \Phi_\Omega^*) + \text{c.c.}] \\ &= i\beta \Omega^{-1} [J(\Phi_\Omega, \partial_x \Phi_\Omega^*) - J(\Phi_\Omega^*, \partial_x \Phi_\Omega)] \\ &= i\beta \Omega^{-1} \partial_x J(\Phi_\Omega, \Phi_\Omega^*), \end{aligned} \quad (50b)$$

where $\bar{\psi}_1^{t_0}$ has been decomposed as follows:

$$\bar{\psi}_1^{t_0} = \bar{\Phi}_1 + \sum_{\Omega \in \mathcal{S}_x} |A_0|^2 \Phi_{\Omega, \Omega^*}, \quad (51)$$

with $\bar{\Phi}_1$ and Φ_{Ω, Ω^*} being real functions.

Note that W_{E1}^{AS} is the asymmetric correction to the first-order symmetric forcing. This asymmetric contribution to the forcing is necessary to provide a growth term in the energy equation since we assumed that the Sverdrup flow is stable (all the basin modes are neutral) on the rapid timescale t_0 . Note that, if the first-order forcing is an harmonic function of y like those used in previous sections, the quadratic contribution is zero.

We also assumed that there is no subharmonic resonances; thus, if Ω is in the spectrum \mathcal{S}_x , 2Ω is not. Collecting the terms proportional to $e^{2i\Omega t_0}$ in (24) yields $(2i\Omega Q + \beta \partial_x) A_1(2\Omega) \Phi_{2\Omega} = -A_0^2(\Omega) J(\Phi_\Omega, \nabla^2 \Phi_\Omega)$. (52)

The biharmonic contribution can thus be summarized as follows:

$$\begin{aligned} A_1(2\Omega, t_1, \dots) &= A_0^2(\Omega) \quad \text{and} \\ \Phi_{2\Omega} &= -\mathcal{L}_{2\Omega}^{-1} J(\Phi_\Omega, \nabla^2 \Phi_\Omega), \end{aligned} \quad (53)$$

where the linear anti-Hermitian operator $\mathcal{L}_{2\Omega}$ is defined by

$$\mathcal{L}_{2\Omega} = 2i\Omega Q + \beta \partial_x. \quad (54)$$

b. Nonlinear amplitude equation

At $O(\epsilon^2)$, the quasigeostrophic equation (3) yields

$$\begin{aligned} \mathcal{L} \psi_2 &= -[\partial_{t_2} Q \psi_0 + \partial_{t_1} Q \psi_1 + J(\psi_0, \nabla^2 \psi_1) \\ &+ J(\psi_1, \nabla^2 \psi_0)]. \end{aligned} \quad (55)$$

The evolution equation for the mode energy $|A_0(\Omega)|^2$ is obtained by two successive solvability conditions to eliminate resonances at timescales t_1 and t_2 . Projecting (55) on Φ_Ω using the scalar product (21), the first prescription yields

$$-\partial_{t_1} A_1 + i|a_1| A_1 - \partial_{t_2} A_0 + b_1 A_0 + b_2 |A_0|^2 A_0 = 0, \quad (56)$$

where the complex numbers $b_1 = b_1' + b_1''$ and $b_2 = b_2' + b_2'' + b_2'''$ are defined as

$$b_1' = (2r)^{-1} \iint_{\mathcal{D}} dx dy \Phi_\Omega^* J(\Phi_\Omega, \nabla^2 \bar{\Phi}_1), \quad (57a)$$

$$b_1'' = (2r)^{-1} \iint_{\mathcal{D}} dx dy \Phi_\Omega^* J(\bar{\Phi}_1, \nabla^2 \Phi_\Omega), \quad (57b)$$

$$b'_2 = (2r)^{-1} \iint_{\mathcal{D}} dx dy \Phi_{\Omega}^* J(\Phi_{\Omega}, \nabla^2 \Phi_{\Omega, \Omega^*}), \quad (57c)$$

$$b''_2 = (2r)^{-1} \iint_{\mathcal{D}} dx dy \Phi_{\Omega}^* J(\Phi_{\Omega, \Omega^*}, \nabla^2 \Phi_{\Omega}), \quad \text{and} \quad (57d)$$

$$b'''_2 = (2r)^{-1} \iint_{\mathcal{D}} dx dy \Phi_{\Omega}^* J(\Phi_{2\Omega}, \nabla^2 \Phi_{\Omega}^*). \quad (57e)$$

A slow evolution equation for the mode energy $E_0 = |A_0|^2$ is derived by summing the product of (56) by A_0^* with its complex conjugate. After integration over time t_1 and some manipulation (integration by parts) one can use (27) to eliminate A_1 terms and finally obtain

$$\partial_{t_2} E_0 = (b_1 + \text{c.c.})E_0 + (b_2 + \text{c.c.})E_0^2. \quad (58)$$

We are thus led to compute the following coefficients:

$$\begin{aligned} (b'_1 + \text{c.c.}) &= (2r)^{-1} \iint_{\mathcal{D}} dx dy \Phi_{\Omega}^* J(\Phi_{\Omega}, \nabla^2 \bar{\Phi}_1) + \text{c.c.} \\ &= -(2r)^{-1} \iint_{\mathcal{D}} dx dy \nabla^2 \bar{\Phi}_1 J(\Phi_{\Omega}, \Phi_{\Omega}^*) + \text{c.c.} = 0, \end{aligned} \quad (59a)$$

since the complex conjugate of the last Jacobian is its opposite and recalling that $\bar{\Phi}_1$ is real from (51);

$$\begin{aligned} (b''_1 + \text{c.c.}) &= (2r)^{-1} \iint_{\mathcal{D}} dx dy \Phi_{\Omega}^* J(\Phi_{\Omega, \Omega^*} + \bar{\Phi}_1, \nabla^2 \Phi_{\Omega}) + \text{c.c.} \\ &= -(2r)^{-1} \iint_{\mathcal{D}} dx dy \bar{\Phi}_1 J(\Phi_{\Omega}^*, \nabla^2 \Phi_{\Omega}) + \text{c.c.} \\ &= -(2r)^{-1} \iint_{\mathcal{D}} dx dy \bar{\Phi}_1 J(\Phi_{\Omega}^*, \text{Bu}^{-1} \Phi_{\Omega} \\ &\quad + \beta i \Omega^{-1} \partial_x \Phi_{\Omega}) + \text{c.c.} \\ &= i(2r)^{-1} \Omega^{-1} \iint_{\mathcal{D}} dx dy \beta (\partial_x \bar{\Phi}_1) J(\Phi_{\Omega}, \Phi_{\Omega}^*), \end{aligned} \quad (59b)$$

which is analogous to the growth rates computed in section 4b at this order of the computation;

$$\begin{aligned} (b'_2 + \text{c.c.}) &= (2r)^{-1} \iint_{\mathcal{D}} dx dy \Phi_{\Omega}^* J(\Phi_{\Omega}, \nabla^2 \Phi_{\Omega, \Omega^*}) + \text{c.c.} \\ &= -(2r)^{-1} \iint_{\mathcal{D}} dx dy \nabla^2 \Phi_{\Omega, \Omega^*} J(\Phi_{\Omega}, \Phi_{\Omega}^*) + \text{c.c.} = 0 \end{aligned} \quad (59c)$$

for reasons similar to those invoked for (59a);

$$\begin{aligned} (b''_2 + \text{c.c.}) &= (2r)^{-1} \iint_{\mathcal{D}} dx dy \Phi_{\Omega}^* J(\Phi_{\Omega, \Omega^*}, \nabla^2 \Phi_{\Omega}) + \text{c.c.} \\ &= -(2r)^{-1} \iint_{\mathcal{D}} dx dy \Phi_{\Omega, \Omega^*} J(\Phi_{\Omega}^*, \nabla^2 \Phi_{\Omega}) + \text{c.c.} \\ &= -(2r)^{-1} \iint_{\mathcal{D}} dx dy \Phi_{\Omega, \Omega^*} J(\Phi_{\Omega}^*, \text{Bu}^{-1} \Phi_{\Omega} \\ &\quad + \beta i \Omega^{-1} \partial_x \Phi_{\Omega}) + \text{c.c.} \\ &= (2r)^{-1} i \Omega^{-1} \iint_{\mathcal{D}} dx dy (\beta \partial_x \Phi_{\Omega, \Omega^*}) J(\Phi_{\Omega}, \Phi_{\Omega}^*) = 0 \end{aligned} \quad (59d)$$

using (50b) for the integration over x , which cancels using boundary conditions; and finally

$$\begin{aligned} (b'''_2 + \text{c.c.}) &= (2r)^{-1} \iint_{\mathcal{D}} dx dy \Phi_{\Omega}^* J(\Phi_{2\Omega}, \nabla^2 \Phi_{\Omega}^*) + \text{c.c.} \\ &= -(2r)^{-1} \iint_{\mathcal{D}} dx dy \Phi_{2\Omega} J(\Phi_{\Omega}^*, \nabla^2 \Phi_{\Omega}^*) + \text{c.c.} \\ &= (2r)^{-1} \iint_{\mathcal{D}} dx dy \Phi_{2\Omega} (\mathcal{L}_{2\Omega} \Phi_{2\Omega})^* + \text{c.c.} = 0, \end{aligned} \quad (59e)$$

since the operator $\mathcal{L}_{2\Omega}$ is anti-Hermitian.

It appears that the growth rate given by (59b) is equivalent to the previously computed $O(\epsilon)$ growth rate (30), purposefully postponed to the order ϵ^2 . Yet, the major concern is that there is no cubic self-saturation, because the terms (59c–e) vanish. These terms cancel out in the energy equation and thus the nonlinearities induce only nonlinear frequency modulation of the form $\Omega + \epsilon^2 \Im(a_1) + \epsilon^2 \Im(b_1) + \epsilon^2 \Im(b_2) |A_0|^2$.

Other modes, higher nonlinearities, and/or explicit dissipative mechanisms are thus required to close the energy budget and saturate the mode spectrum.

7. Discussion and conclusions

Using a weakly nonlinear expansion, we studied the nonlinear interactions involving Rossby basin modes and the mean flow for a one-layer reduced-gravity quasi-geostrophic model for different values of the Burger number (Bu). Analytical calculations were performed in the no-surface-deviation case (Bu = ∞), while the more relevant cases (Bu \ll 1) were treated numerically.

We found that basin modes are unstable for particular meridional gyre configurations associated with a single harmonic of the zonally invariant Ekman pumping. Instability occurs when the gradient of relative vorticity associated with this gyre alternation is opposed to the planetary vorticity gradient β . The meridional scale of

the unstable mode is then 2 times that of the Ekman pumping. Because of its limited oceanographic relevance, the reversed double-gyre case is not very popular in the literature, and so we could not confirm our theoretical stability prediction. However, Colin de Verdière (1977) reports from double-gyre laboratory experiments on a fundamentally different stability behavior depending on gyre configuration when the nonlinearity parameter ϵ becomes of order 1, which may support our result. From isolated source–sink flow experiments in a sliced cylinder geometry on a rotating table β plane, he concludes “When the source is south and the sink north, the flow is absolutely stable and intense steady circulation can be induced. On the other hand, the reverse configuration when the sink is south and the source north leads to an instability of the flow as soon as $U/(\beta L^2)$ is order one” (see his figure on p. 164). From numerical experiments in the highly nonlinear Fofonoff regime, Griffa and Salmon (1989) also found different stability property of regular and reversed wind-driven gyres, but in their case it is the regular configuration that is unstable.

Such a reversed gyre configuration might be of interest in the Tropics (P. Cessi 2002, personal communication) but also, as pointed out by an anonymous reviewer, more generally through midlatitude western boundary currents in which circulation opposed to the interior Sverdrup flow may feed the growth of perturbations near recirculation gyres.

We have also shown that basin subharmonic instability can occur. For large-scale reduced-gravity modes ($Bu \ll 1$) this leads to the excitation of the low-frequency part of the spectrum that coincides with the modes with the largest zonal wavelength. We discussed this potential mechanism for spectral reddening in the context of the Cessi and Paparella (2001) numerical experiments.

We also investigated the nonlinear self-saturation of an isolated mode. Unfortunately, it appears that cubic nonlinearities cannot close the energy budget, suggesting that higher-order nonlinearities and/or other modes must come into play to equilibrate the growth of the unstable modes.

The suitability of a weakly nonlinear expansion having been assessed in this simple one-layer model, the next step is under way to consider basin modes and mean flow interactions in multilayer models in which the baroclinic mode structure can be influenced by the barotropic mean flow advection (Spydell and Cessi 2003) and baroclinic instability can occur.

Acknowledgments. Computational facilities were provided by the Institut du Développement et des Ressources en Informatique Scientifique (IDRIS, Orsay, France). We are very grateful to A. Colin de Verdière for insightful discussions and comments and to the anonymous reviewers for very thorough and careful

suggestions that helped us to clarify (we hope enough) the manuscript.

REFERENCES

- Cessi, P., and G. R. Ierley, 1995: Symmetry-breaking multiple equilibria in quasigeostrophic, wind driven flows. *J. Phys. Oceanogr.*, **25**, 1196–1205.
- , and S. Louazel, 2001: Decadal oscillation response to stochastic wind forcing. *J. Phys. Oceanogr.*, **31**, 3020–3029.
- , and F. Paparella, 2001: Excitation of basin modes by ocean–atmosphere coupling. *Geophys. Res. Lett.*, **28**, 2437–2440.
- , and F. Primeau, 2001: Dissipative selection of low-frequency modes in a reduced-gravity basin. *J. Phys. Oceanogr.*, **31**, 127–137.
- Colin de Verdière, A., 1977: Quasigeostrophic flows and turbulence in a rotating homogeneous fluid. Ph.D. thesis, MIT–WHOI Joint Program, 173 pp.
- , and T. Huck, 1999: Baroclinic instability: An oceanic wave-maker for interdecadal variability. *J. Phys. Oceanogr.*, **29**, 893–910.
- Delworth, T. L., and R. J. Greatbatch, 2000: Multidecadal thermohaline circulation variability driven by atmospheric surface flux forcing. *J. Climate*, **13**, 1481–1495.
- , S. Manabe, and R. J. Stouffer, 1993: Interdecadal variations of the thermohaline circulation in a coupled ocean–atmosphere model. *J. Climate*, **6**, 1993–2011.
- Dijkstra, H. A., 2000: *Nonlinear Physical Oceanography: A Dynamical Systems Approach to the Large Scale Ocean Circulation and El Niño*. Vol. 22, Kluwer Academic, 480 pp.
- , and C. A. Katsman, 1997: Temporal variability of the wind driven quasigeostrophic double gyre ocean circulation: Basic bifurcation diagrams. *Geophys. Astrophys. Fluid Dyn.*, **85**, 195–232.
- Fauve, S., 1998: Pattern forming instabilities. *Hydrodynamics and Nonlinear Instabilities*, C. Godrèche and P. Manneville, Eds., Cambridge University Press, 387–491.
- Flierl, G. R., 1977: Simple application of McWilliams “A note on a consistent quasigeostrophic model in a multiply connected domain.” *Dyn. Atmos. Oceans*, **1**, 443–453.
- Greatbatch, R. J., and S. Zhang, 1995: An interdecadal oscillation in a idealized ocean basin forced by constant heat fluxes. *J. Climate*, **8**, 81–91.
- Griffa, A., and R. Salmon, 1989: Wind-driven ocean circulation and equilibrium statistical mechanics. *J. Mar. Res.*, **47**, 457–492.
- Jiang, S., F.-F. Jin, and M. Ghil, 1995: Multiple equilibria and aperiodic solutions in a wind-driven double gyre, shallow-water model. *J. Phys. Oceanogr.*, **25**, 764–786.
- Kushnir, Y., 1994: Interdecadal variations in North Atlantic sea surface temperature and associated atmospheric conditions. *J. Climate*, **7**, 141–157.
- Lehouck, R. B., D. C. Sorensen, and C. Yang, 1998: ARPACK users’ guide: Solution of large scale eigenvalue problems with implicitly restarted Arnoldi methods. SIAM, 160 pp. [Available online from <http://www.caam.rice.edu/software/ARPACK/>.]
- Longuet-Higgins, M. S., 1964: Planetary waves on a rotating sphere. *Proc. Roy. Soc. London*, **279A**, 446–473.
- Mann, M. E., R. S. Bradley, and M. K. Hughes, 1998: Global-scale temperature patterns and climate forcing over the past six centuries. *Nature*, **392**, 779–787.
- McWilliams, J. C., 1977: A note on a consistent quasigeostrophic model in a multiply connected domain. *Dyn. Atmos. Oceans*, **1**, 427–441.
- Nayfeh, A. H., 1993: *Introduction to Perturbation Techniques*. Wiley-Interscience, 519 pp.
- Pedlosky, J., 1987: *Geophysical Fluid Dynamics*. 2d ed. Springer-Verlag, 710 pp.
- , 1996: *Ocean Circulation Theory*. Springer-Verlag, 453 pp.
- Sheremet, V. A., G. R. Ierley, and V. M. Kamenkovich, 1997: Ei-

- genanalysis of the two-dimensional wind-driven circulation problem. *J. Mar. Res.*, **55**, 57–92.
- Simonnet, E., and H. A. Dijkstra, 2002: Spontaneous generation of low-frequency modes of variability in the wind-driven ocean circulation. *J. Phys. Oceanogr.*, **32**, 1747–1762.
- Speich, S., H. A. Dijkstra, and M. Ghil, 1995: Successive bifurcations of a shallow water model with applications to the wind driven circulation. *Nonlinear Proc. Geophys.*, **2**, 241–268.
- Spydell, M., and P. Cessi, 2003: Baroclinic modes in a two-layer basin. *J. Phys. Oceanogr.*, **33**, 610–622.
- Strogatz, S. H., 1994: *Nonlinear Dynamics and Chaos*. Addison-Wesley, 498 pp.